Zeeman-Induced Valley-Sensitive Photocurrent in Monolayer MoS$_2$

Xiao-Xiao Zhang,[1,2] You Lai,[3,4] Emma Dohner,[5] Seongphill Moon,[3,4] Takashi Taniguchi,[6]
Kenji Watanabe,[6] Dmitry Smirnov,[4] and Tony F. Heinz[1,2,*]

[1]*Department of Applied Physics, Stanford University, Stanford, California 94305, USA*
[2]*SLAC National Accelerator Laboratory, 2575 Sand Hill Road, Menlo Park, California 94025, USA*
[3]*Department of Physics, Florida State University, Tallahassee, Florida 32306, USA*
[4]*National High Magnetic Field Laboratory, Tallahassee, Florida 32310, USA*
[5]*Department of Chemistry, Stanford University, Stanford, California 94305, USA*
[6]*National Institute for Materials Science, 1-1 Namiki, Tsukuba 305-0044, Japan*

The control of the valley degree of freedom lies at the core of interest in monolayer transition metal dichalcogenides, where specific valley-spin excitation can be created using circularly polarized light. Measurement and manipulation of the valley index has also been achieved, but mainly with purely optical methods. Here, in monolayer MoS$_2$, we identify a response to the valley polarization of excitons in the longitudinal electrical transport when the valley degeneracy is broken by an out-of-plane magnetic field B_z. The spin information is also simultaneously determined with spin-sensitive contacts. In the presence of B_z, a significant modulation of the photocurrent is observed as a function of the circular polarization state of the excitation. We attribute this effect to unbalanced transport of valley-polarized trions induced by the opposite Zeeman shifts of two (K and K') valleys. Our interpretation is supported by the contrasting behavior in bilayer MoS$_2$, as well as the observed doping and spatial dependence of the valley photocurrent.

Special interest in the 2D semiconductors in the transition metal dichalcogenide (TMDC) family arises from the possibility of ready optical access to the valley index, the pseudospin degree of freedom associated with the presence of degenerate K or K' valleys in the Brillouin zone [1,2]. Under near-resonant excitation conditions, circularly polarized light selectively creates excitons in a specific valley [1,3–6]. Together with the valley-spin coupling, the resulting excited carriers are both valley and spin polarized. Extensive work has been performed to explore various optical methods to generate, monitor [7,8], and manipulate [9] valley information based on excitons in TMDCs. On the other hand, for more flexible valleytronic devices, it is essential to understand how the valley polarization of excitons affects the optoelectronic response. Previous studies have shown that the valley Hall effect contributes to a transverse voltage [10], but the more conventional response of the *longitudinal* photocurrent remains largely unexplored.

Here, we demonstrate the existence of a valley-sensitive photocurrent in monolayer MoS$_2$ when an out-of-plane external magnetic field is applied to lift the valley degeneracy. From the photocurrent's dependence on the magnetic-field strength, we are able to identify components related to spin- and valley-polarized excitation. In monolayer samples, in addition to a spin-sensitive signal detected with ferromagnetic contacts, we observe a significant valley-polarized response which increases linearly with the out-of-plane magnetic field B_z. We have further characterized the dependence of the photocurrent on the doping level, as well as the spatial profile of the valley-selective photocurrent. The experimental data support an explanation of the valley-sensitive optoelectronic response as originating from the valley-polarized trions, the result of the presence of the valley-polarized free carriers from the Zeeman effect. Our results establish a robust method for electrically extracting information about the valley degree of freedom of optical excitation in the monolayer TMDCs, thus providing a crucial bridge between the optical and electrical properties of valleytronic devices. We have measured photocurrent in MoS$_2$ crystals from the monolayer to few-layer thickness. To create valley-polarized excitons, we excited the system with circularly polarized laser radiation at a photon energy near the A exciton resonance, as shown in Fig. 1(c). The laser radiation was switched between left and right circularly polarized ($\sigma + /\sigma-$) states with either a liquid crystal retarder or a half-wave plate, in combination with a quarter-wave plate [Fig. 1(b)]. Spin-selective electrical contacts for the photoconductivity measurements were prepared on the MoS$_2$ samples using a ferromagnetic metal (Co) with a ~1 nm TiO$_2$ tunneling barrier. Typical current-voltage characteristics of the photoresponse from monolayer MoS$_2$ are shown in Fig. 1(e). Both the total photocurrent, $I_{\text{total}} = (I_{\sigma+} + I_{\sigma-})/2$, as measured at the laser chopping frequency, and the polarization-dependent photocurrent,
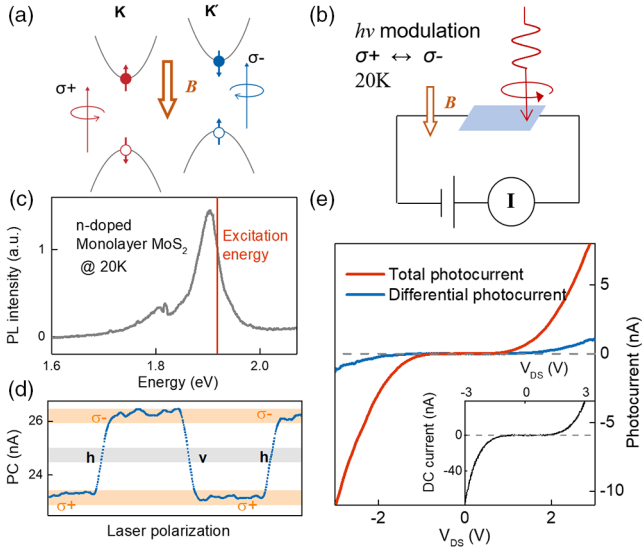
FIG. 1. (a) Band structure of monolayer MoS_2 near the K and K' valleys, showing the valley-spin optical selection rule for circular polarized light. An out-of-plane magnetic field B_z breaks the energy degeneracy and shifts the two valleys in opposite directions. (b) The photocurrent is measured under B_z for an applied bias voltage V_{DS}. The polarization state of the light is switched between opposite circular polarization states. The total and differential photocurrent are recorded simultaneously. (c) The measured PL spectrum for monolayer MoS_2 is capped by h-BN at $T = 20$ K and $B_z = 0$, showing dominant emission from n-type trions at 1.92 eV. The red line corresponds to the photon energy of the excitation laser for the photocurrent measurements. (d) Typical variation of the photocurrent under a magnetic field as the light polarization went through circularly polarized $\sigma+$, horizontally polarized h, circularly polarized $\sigma-$, vertically polarized, v and back to $\sigma+$. (e) Typical I-V characteristics of the total photocurrent (red) and differential photocurrent (blue) for $B_z = 15$ T. (Inset) The corresponding I-V characteristics of the dark device.

FIG. 2. (a) The polarization P of the photocurrent plotted as a function of the magnetic field for monolayer MoS_2 (n type) with ferromagnetic contacts. Two distinct regimes of response can be seen. (b) The corresponding magnetic-field dependence of P for monolayer MoS_2 with Au contacts, and (c) bilayer MoS_2 ($2H$, n type) with ferromagnetic contacts.

$I_{\text{diff}} = (I_{\sigma+} - I_{\sigma-})/2$, as measured at the polarization alternating frequency, are presented. $I_{\sigma+}$ and $I_{\sigma-}$ correspond, respectively, to the photocurrent under $\sigma+$ and $\sigma-$ polarized light. The bias dependence of the dc current [inset of Fig. 1(e)] exhibits the behavior expected for Schottky junction contacts. Unless otherwise specified, in this Letter we discuss only the photocurrent, typically measured at a bias of $V_{DS} = 3$ V and a sample temperature of 20 K.

We focused on measuring the modulation of photocurrent induced by the circular polarization state of the excitation, defining $P = (I_{\sigma+} - I_{\sigma-})/(I_{\sigma+} + I_{\sigma-})$ to quantify the fractional change. Figure 2(a) summarizes the main results for the magnetic-field dependence of P for monolayer MoS_2 with ferromagnetic contacts, which increases significantly with increasing field. The measured P reflects only the effects from the circular polarization of excitation. As can be seen from Fig. 1(d), the different linearly polarized states (h/v) induce little change in the magnitude of photocurrent, in contrast to photogalvanic measurements
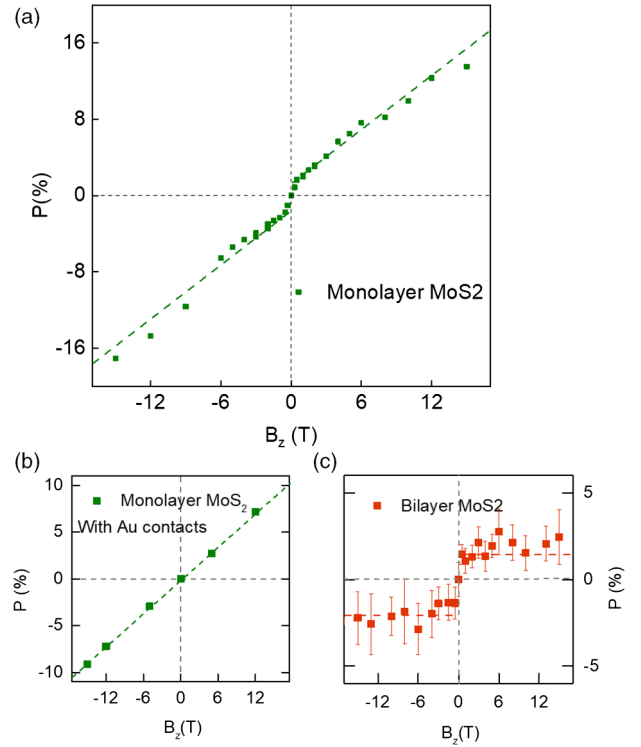
under oblique optical excitation [11,12]. The dependence of P on the magnetic field exhibits two distinct regimes. There is a sharp turn-on at low B_z (region I), followed by a slower steady increase (region II), up to $P = 18\%$ for the highest B_z. We also obtained data for another monolayer MoS_2 sample exhibiting a weaker modulation in region II, and a correspondingly more pronounced delineation of the two regions (see the Supplemental Material [13]).

The origin of the initial rapid rise in P in region I is the spin-selective tunneling into the ferromagnetic contacts. As mentioned above, circularly polarized resonant excitation can optically select the spin of the photoexcited carriers. Near the electrical contacts, the large built-in electric field induces dissociation of photogenerated excitons into spin-polarized carriers. The carriers are collected by the ferromagnetic contacts, with different efficiencies depending on the relative spin alignment with the contacts. Under a weak magnetic field [~0.5 T in Fig. 2(a)], the original in-plane magnetic polarization in ferromagnetic contacts becomes fully aligned along the z direction, resulting in the fast onset of spin-dependent photocurrent, leading to $P \sim 2\%$. The lack of hysteresis reflects the in-plane easy axis of the contacts [20]. Similar results, with higher values of spin polarization, have been reported previously for p-type monolayer WS_2 [21,22]. The spin selectivity of the

detection process depends on the thickness and quality of the tunneling junction [23] and requires optimization to obtain a high polarization.

The more intriguing and unexpected behavior is the nonsaturating increase of P with field in region II in Fig. 2(a). To investigate its origin, we measured monolayer MoS_2 with gold (nonferromagnetic) contacts. As shown in Fig. 2(b), the variation of the photocurrent with polarization state also exhibited a comparable quasilinear increase with magnetic field. This result reveals that, unlike the previous discussion of spin signal, the emergence of P arises from the *intrinsic* response of the TMDC layer under the out-of-plane magnetic field. The linear dependence to the applied B_Z is also suggestive of a connection to Zeeman energy shift between the K and K' valleys.

The circular polarization of the excitation influences the valley and spin states of photogenerated carriers. To further reveal the specific role of the valley index, as opposed to the spin index, we performed the same measurements on bilayer $2H$-MoS_2 samples with ferromagnetic contacts (in the Supplemental Material [13], we include the results for bilayers with gold contacts). Unlike the monolayer, the $2H$-stacked MoS_2 bilayer exhibits inversion symmetry. This leads to equal excitation of both valleys by circularly polarized light, but retention of the spin selectivity. In strong contrast to the case of monolayers, the photoresponse of the bilayer sample in Fig. 2(c) exhibits little variation in region II (typically $<5\%$ for all tested bilayers), while still showing similar spin-selective excitation results in region I.

From the above, we infer that the significant polarization dependence of the photocurrent observed in region II is indeed associated with the valley index in the monolayer material. In analyzing the underlying mechanism, we first note that this effect does not arise simply from the light absorption difference due to Zeeman splitting of K and K' valley excitons. Although the light absorption does acquire a polarization dependence from the shift of excitonic resonances, the slight Zeeman shift and broad exciton linewidth ($\sim$40 meV) indicate that this effect is too weak to account for the observed large modulation in the photocurrent. In the Supplemental Material [13], we present our measurements on the Zeeman shift of excitonic features and provide a more detailed estimation of such an absorption difference.

The more significant effect arising from the Zeeman shift involves the role of free carriers present in the material from doping. Since the Zeeman shifts of the two valleys are large compared to the thermal energy, the relative carrier populations in the two valleys can be strongly modified by the applied magnetic field. Note that we neglect the potential formation of Landau levels here. The low mobility of carriers in the sample leads to a scattering rate that is much higher than the carrier cyclotron frequency. The field-induced imbalance in free carrier population in the two

valleys affects the formation of charged excitons—the trion states. For the most stable trion configuration, the two electrons or holes forming n/p-type trions have opposite spin [24]. If we initially create equal concentrations of excitons in the two valleys, the relative abundance of free carriers in, say, the K valley under the magnetic field, as depicted in Fig. 3(c) for the case of n doping, will lead to a higher probability of forming K' valley trions. Such a valley-selective trion formation under B_z has previously been reported in magneto-PL measurements [12,25] and was also observed in our complementary magneto-PL measurement presented in the Supplemental Material [13]. We attribute our observed valley-dependent photocurrent response to the role of valley-polarized trions, as we discuss below in greater detail.

Strong evidence supporting the role of trions in the valley-dependent photocurrent comes from the doping dependence of the effect. Within our picture, the most pronounced valley selection for trion formation should occur for the moderate doping condition illustrated in Fig. 3(c), favoring trions in the K' valley and neutral excitons in K valley. At higher doping density, essentially all of the absorbed photons will be converted into trions,
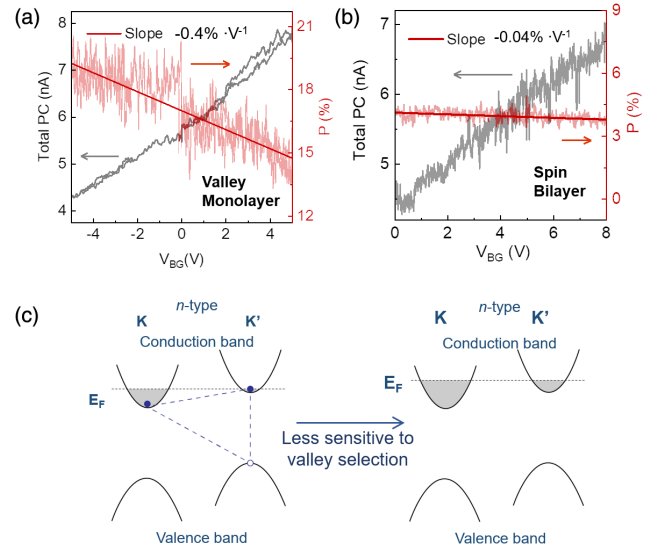
FIG. 3. (a) Doping dependence of the total photocurrent (gray) and polarization dependency P (red) for a monolayer sample at $B_z = 17.5$ T. The P reflects mostly the valley characteristics and decreases with higher doping. (b) For a bilayer ($2H$) sample at 17.5 T, the total photocurrent has a similar n-type doping dependence for these two samples, while the spin photocurrent polarization shows much smaller doping dependence. (c) Under the applied B_Z, K and K' valleys shift in opposite directions. For the plotted case of n-type MoS_2 samples, it creates a higher density of K valley free electrons, which then favors the formation of K' valley trions (shown as the dashed-line connected quasiparticle). When further increasing the doping level, free electrons are available in both valleys, decreasing the selective formation of K' valley trions.

irrespective of the valley in which they are created; we then would no longer expect a significant polarization dependence of the photocurrent. Indeed, as shown in Fig. 3(a), we see a decrease of the valley-dependent P when further increasing the carrier concentration of the n-doped monolayer sample. Here, we consider the expected effect more quantitatively. The measured sample was estimated to be electron photodoped to a level of $\sim 3 \times 10^{12}/\text{cm}^2$. For an effective electron mass of $\sim 0.45 m_e$ [26], the Fermi level then lies ~ 7 meV above the conduction band minimum, under the assumption of fourfold degeneracy for the slightly spin-split conduction bands (CBs) in monolayer MoS$_2$ [26]. Under the relevant applied magnetic field of 17.5 T, the CBs in the K/K' valleys are expected to shift by ± 2.3 meV, respectively, based on the g-factor estimation presented in the Supplemental Material [13]. This shift of the bands leads to a fractional change in the electron density in the two valleys of approximately 33%, large enough to explain the significant value ($P = 16\%$) measured for the polarization dependence of the photocurrent. When the gate voltage changed from -5 V to 5 V, the fractional difference in the valley electron density drops from 37% to 30%, with the observed P decreasing from 19% to 15% [Fig. 3(a)], consistent with our picture of the importance of the valley charge imbalance. On the other hand, the spin-polarized component of the response detected by the ferromagnetic contacts is not expected to exhibit any strong doping dependence. This is confirmed in the bilayer data in Fig. 3(b). We see minimal change in spin-selective photocurrent, while the total photocurrent exhibits a similar doping dependence to that of the monolayer shown in Fig. 3(a).

The spatial profile of valley photocurrent further reveals the connection of the photocurrent valley sensitivity to trion transport. Figures 4(a) and 4(b) compare the valley- and spin-selective components of the photocurrent as a function of the spatial position of the laser spot on the device. The total photocurrent is found to be higher near the source contact where more pronounced band bending is present [27] [Fig. 4(c)]. This behavior is expected for the generation of photocurrent in a material that requires dissociation of the strongly bound excitons under the effective electric field produced by the Schottky barrier. Near the drain, due to the large applied voltage (3 V) compared to a typical Schottky junction height (of ~ 0.2 eV [28]), the material is expected to have flatter bands, with diffusive exciton transport dominating. While the spin-polarized photocurrent is found to follow the spatial profile of the total photocurrent, the valley-dependent component peaks at the *opposite* end of the device. (Note that, in order to record both the spin and valley signals in Fig. 2, the position of the laser illumination was chosen between the two electrodes.) This peculiar profile is consistent with the expected transport contribution from trions. For the relevant case of n-type trions, the built-in electric field
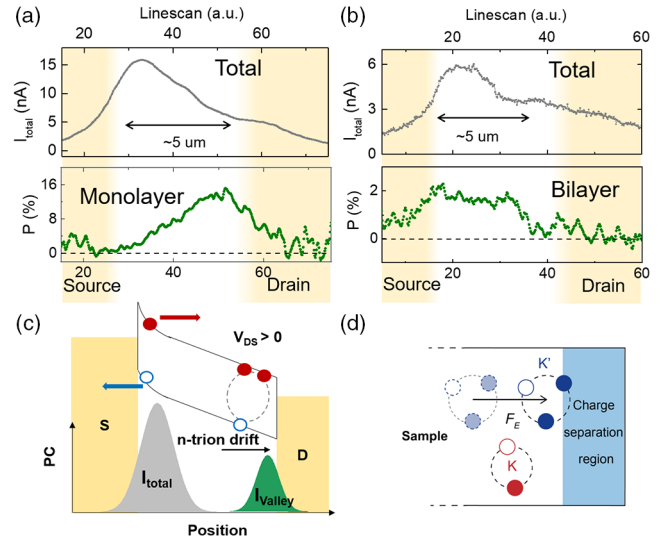

FIG. 4. (a) Spatial distribution of photocurrent across the source and drain contacts for monolayer sample at 16 T. The gray line in The upper panel indicates the total photocurrent distribution. The nonzero tails at the ends of the contacts are due to the large laser spot (~ 2 μm) and residual scattered light. The corresponding polarization P, which comes mainly from the valley contribution, is plotted in the lower panel in green. (b) The same measurements and notations as (a) measured in bilayer MoS$_2$. The spatial distribution for P now mainly reflects the spin polarization contribution. (c) Schematics of the material's bands across the device at the given experimental condition (n doping, $V_{DS} > 0$). The band near the source has a higher band bending. Correspondingly, we have a higher $I_{\text{total}}n$ near the source contact, as indicated by the gray area. The applied electric field would drift the valley-polarized n trions towards drain contacts, creating a higher valley photocurrent denoted in green. (d) Schematics for the transport scenario comparing the trions and neutral excitons of different valleys.

causes the trions to drift towards the drain contact, but the same effect is absent at the opposite contact. The observed spatial dependence of the valley-sensitive photocurrent thus strongly suggests the role of the drift current from valley-polarized trions.

In considering the role of trions in the valley photocurrent, we note that since excitons in monolayer TMDC are tightly bound, only a fraction of the excitons created near the contact are expected to be dissociated and to contribute to photocurrent. As schematically shown in Fig. 4(d), on the side of the device where we observed the valley photocurrent, neutral excitons will reach contacts only by diffusion, typically over a few nanometers, while trions transport will be assisted by the built-in electric field (the Supplemental Material [13] includes a quantitative discussion of the relevant parameters). Thus, the observed photocurrent valley sensitivity can occur through the creation of valley-polarized trions in the presence of B_z, as free charges populate one valley more strongly. For the bands illustrated in Fig. 3(c), excitons in the K' valley relax

into trions, while excitons in the K valley remain electrically neutral. This gives rise to increased photocurrent when exciting the K' valley due to extra trion drift current. The Berry curvature of Bloch electrons is also expected to contribute to a valley-dependent photocurrent under the out-of-plane magnetic field [29], but with a more homogeneous spatial distribution. Finally, we would like to discuss the impact of absorption from the occupancy of valley-polarized free electrons. Since the photon energy for our excitation is close to the neutral exciton and trion resonances, the absorption of $\sigma+/\sigma-$ photons might be different because the two valleys have different doping levels in the presence of the magnetic field. Such a doping-induced absorption change would have been most significant when the sample is close to charge neutrality. Under our experimental conditions of moderately doped ($\sim 3 \times 10^{12}/cm^2$) samples, this absorption difference is expected to be minor (see, e.g., corresponding region in previous reflection measurements by Wang *et al.* [30]). Furthermore, our measured valley polarization of photocurrent shows a clear decay when moving the laser excitation away from the contact, which would not be expected from the more uniform difference in absorption. Finally, such doping-dependent absorption would be very sensitive to the excitation photon energy with respect the exciton resonance. Several samples with slightly different resonance energies, due to strain or different dielectric environment, exhibited similar results, again indicating that the mechanism can be attributed to the trion drift current. Future studies in which the laser photon energy is systematically varied would help to disentangle these two mechanisms.

In summary, we have isolated and characterized a valley-dependent contribution to the photocurrent in atomically thin MoS_2, which increases linearly with increasing out-of-plane magnetic field. We explain this phenomenon as originating from the valley-selective formation of trions induced by the transfer of free charges between valleys under the magnetic field. The distinctly different spatial and doping dependences of the spin- and valley-polarized photocurrent reveal the role of a drift transport contribution from trions and support our proposed mechanism. Unlike the strict conditions required by many other electrical methods, e.g., high mobilities for the valley Hall effect or high-quality spin filtering contacts, this method is relatively robust and easy to implement as an effective way to read out optically imprinted valley information. By interfacing with layered ferromagnetic insulators like EuS [31] and CrI_3 [32], the large effective magnetic field from the ferromagnetic substrate should permit us to eliminate the need for any strong external magnetic field, facilitating the convenient implementation of this scheme in practical device geometries.

*corresponding author.
tony.heinz@stanford.edu

[1] D. Xiao, G.-B. Liu, W. Feng, X. Xu, and W. Yao, Phys. Rev. Lett. **108,** 196802 (2012).
[2] X. Xu, W. Yao, D. Xiao, and T. F. Heinz, Nat. Phys. **10,** 343 (2014).
[3] T. Cao *et al.*, Nat. Commun. **3,** 887 (2012).
[4] A. M. Jones *et al.*, Nat. Nanotechnol. **8,** 634 (2013).
[5] K. F. Mak, K. He, J. Shan, and T. F. Heinz, Nat. Nanotechnol. **7,** 494 (2012).
[6] H. Zeng, J. Dai, W. Yao, D. Xiao, and X. Cui, Nat. Nanotechnol. **7,** 490 (2012).
[7] P. Dey, L. Yang, C. Robert, G. Wang, B. Urbaszek, X. Marie, and S. A. Crooker, Phys. Rev. Lett. **119,** 137401 (2017).
[8] L. Yang, N. A. Sinitsyn, W. Chen, J. Yuan, J. Zhang, J. Lou, and S. A. Crooker, Nat. Phys. **11,** 830 (2015).
[9] Z. Ye, D. Sun, and T. F. Heinz, Nat. Phys. **13,** 26 (2016).
[10] K. F. Mak, K. L. McGill, J. Park, and P. L. McEuen, Science **344,** 1489 (2014).
[11] M. Eginligil, B. Cao, Z. Wang, X. Shen, C. Cong, J. Shang, C. Soci, and T. Yu, Nat. Commun. **6,** 7636 (2015).
[12] H. Yuan *et al.*, Nat. Nanotechnol. **9,** 851 (2014).
[13] See Supplemental Material at http://link.aps.org/supplemental/10.1103/PhysRevLett.122.127401, which includes Refs. [14–19], for experimental methods, the optical characterization of the sample, and further discussions.
[14] C.-C. Wu, D. Jariwala, V. K. Sangwan, T. J. Marks, M. C. Hersam, and L. J. Lauhon, J. Phys. Chem. Lett. **4,** 2508 (2013).
[15] H. Yamaguchi *et al.*, ACS Nano **9,** 840 (2015).
[16] A. Sekine and A. H. MacDonald, Phys. Rev. B **97,** 201301 (2018).
[17] Z. Wang, L. Zhao, K. F. Mak, and J. Shan, Nano Lett. **17,** 740 (2017).
[18] C. Zhao *et al.*, Nat. Nanotechnol. **12,** 757 (2017).
[19] D. Zhong *et al.*, Sci. Adv. **3,** e1603113 (2017).
[20] J. Lee, K. F. Mak, and J. Shan, Nat. Nanotechnol. **11,** 421 (2016).
[21] A. V. Stier, K. M. McCreary, B. T. Jonker, J. Kono, and S. A. Crooker, Nat. Commun. **7,** 10643 (2016).
[22] Y. Li *et al.*, Phys. Rev. Lett. **113,** 266804 (2014).
[23] D. Xiao, W. Yao, and Q. Niu, Phys. Rev. Lett. **99,** 236809 (2007).

[24] A. Chernikov, A. M. van der Zande, H. M. Hill, A. F. Rigosi, A. Velauthapillai, J. Hone, and T. F. Heinz, Phys. Rev. Lett. **115**, 126802 (2015).

[25] Z. Wu *et al.*, Nat. Commun. **7**, 12955 (2016).

[26] S. Blundell, *Magnetism in Condensed Matter* (Oxford University Press, Oxford, 2003).

[27] L. Xie and X. Cui, Proc. Natl. Acad. Sci. U.S.A. **113**, 3746 (2016).

[28] X. Chen, T. Yan, B. Zhu, S. Yang, and X. Cui, ACS Nano **11**, 1581 (2017).

[29] G. Schmidt, D. Ferrand, L. W. Molenkamp, A. T. Filip, and B. J. van Wees, Phys. Rev. B **62**, R4790 (2000).

[30] T. C. Berkelbach, M. S. Hybertsen, and D. R. Reichman, Phys. Rev. B **88**, 045318 (2013).

[31] D. MacNeill, C. Heikes, K. F. Mak, Z. Anderson, A. Kormányos, V. Zólyomi, J. Park, and D. C. Ralph, Phys. Rev. Lett. **114**, 037401 (2015).

[32] A. Kormányos, G. Burkard, M. Gmitra, J. Fabian, V. Zólyomi, N. D. Drummond, and V. Fal'ko, 2D Mater. **2**, 022001 (2015).